

The Influence of Multiwall Carbon Nanotubes Additives on the Structural and Mechanical Properties of Alumina Composites

Abdulsattar K. Hasan^a, Thamir A. Jumah^a and Kassim M. Wadi^b

^a Department of Physics, College of Science, Al-Nahrain University, Jadiriya, Baghdad, Iraq.

^b Almamon College, Bagdad, Iraq.

Doi: <https://doi.org/10.47011/18.1.7>

Received on: 16/09/2023;

Accepted on: 26/11/2023

Abstract: Monolithic Al₂O₃ / multi-walled carbon nanotube (MWCNT) composites were generated in three categories through ratios by conventional sintering method. The microstructure and mechanical properties were studied. After being prepared and pressed, the specimens were sintered. The as-synthesized specimens were characterized through XRD, SEM, particle size distribution, and porosity measurements. The mechanical property evaluations included measuring the compression, Vickers hardness, and Charpy impact testing. The absorbed energy and toughness were calculated for each sample. The XRD patterns were used to identify the structural parameters of the samples and identify the phases present. The SEM images were used to investigate the dispersion characteristics of the MWCNTs in addition to the nature of the fractured areas. The results show the possibility of enhancing the mechanical properties of the composite material by varying the composition ratio of the MWCNTs. The mechanical properties are also varying with the porosity character of the samples. The present analysis of the mechanical and structural properties of the fabricated samples is believed to assist the development of the composite material for armor applications.

Keywords: Ceramics composites, MWCNTs, Microstructure, Armors, Mechanical properties.

1. Introduction

The number of fields in which ceramics can be used is increasing significantly due to advancements in ceramic-based nanocomposites (CMNCs) [1]. Alumina (Al₂O₃)-based compounds are prospective engineering materials with exceptional mechanical and tribological characteristics. Due to their chemical inertness and hardness, ceramics are now widely used in applications such as armor, dental implants, high-speed cutting tools, electrical and chemical insulators, wear-resistant parts, and various coatings. Ceramics are known to have excellent thermal and electrical insulating qualities [2-6]. Monolithic porcelain has low

fracture toughness, weak creep resistance, and intrinsic brittleness. Over the past few decades, numerous attempts have been made to create ceramic matrix composites (CMCs), which possess superior mechanical properties over monolithic ceramics [7]. Due to their light weight, excellent toughness, and exceptional thermal and chemical resistance, CMCs have recently been a popular choice for a variety of applications [8]. The use of nano-fillers as a reinforcing phase is an important and promising strategy for improving the mechanical characteristics of CMNCs [1]. As prospective nano-fillers for CMNCs, carbon nanotubes

(CNTs) have come to light [9-13]. The reinforced alumina composites cannot, however, be guaranteed to perform as envisaged despite the remarkable characteristics of CNTs. The primary explanation is that the mechanical properties of CNTs and their reinforced composites are significantly influenced by interfacial features [14, 15]. In the present study, Al₂O₃-MWCNT composites are developed with the use of multi-walled carbon nanotubes (MWCNTs). MWCNTs have an approximate density of 2.6 g/cm³ and a specific surface area of 200–400 m²/g. MWCNTs have compression strength between 10 and 60 GPa and a modulus between 0.3 and 1 TPa. Additionally, MWCNTs possess a high thermal conductivity of up to 3000 W/m and a noteworthy electrical conductivity in the range of 106-107 S/m [16, 17].

As a result of its striking high hardness (15-22 GPa), chemical inertness, and strong oxidation resistance, Al₂O₃ ceramics is one of the important, widely used ceramic materials [18]. Al₂O₃ ceramics is one of the cheapest and commercially viable options used in material engineering. Al₂O₃ has a density between 3.75 and 3.95 gm/cm³ and a melting point of 2071 °C [19]. In addition to these characteristics, the material has a bulk modulus of 324 GPa, a Young's modulus of 413 GPa, and a compressive strength between 2000 and 4000 MPa. Al₂O₃ has a 5 MPa/m fracture toughness and a 10.9 10⁻⁶/K thermal expansion coefficient [19]. Despite having a number of exceptional functional qualities, Al₂O₃'s applications are restricted due to its low fracture toughness. To overcome this limitation, significant efforts have been made to enhance the fracture toughness of Al₂O₃ using advanced sintering techniques such as spark plasma sintering (SPS) and the incorporation of nano-fillers. [20, 21]. The target of this project is to study the structural variations and mechanical properties of composites reinforced with carbon nanotubes, aiming to improve their performance for armor applications.

2. Materials and Methods

2.1. Preparation of Alumina-MWCNT Composites

Due to their high tendency to agglomerate, MWCNTs are not easily distributed homogeneously in the matrix material of the reinforced composite. This challenge arises from

the morphological and structural aspects of the CNTs. Accordingly, the interface between the MWCNTs and the matrix may not be well constructed. To transfer/generate the appropriate mechanical and structural properties to the compounds, the dispersion of MWCNTs inside the matrix must be as homogenous as feasible.

The starting materials were initially weighed accurately and added to the ball mill container. The ball milling was achieved in a wet medium in the presence of ethanol. Materials are constantly ground by a motor-driven mill with atria-stabilized zirconia balls as grinding media for the homogeneous mixing of powders for 24 hours. Then, the mixture was dried for 30 minutes at 100°C in a vacuum oven. 2wt% PVA and polyvinyl alcohol were added as binders to the dried material and crushed using a mortar and pestle for further mixing. Before sintering, the combined mixture was pressed unidirectional into 12 mm diameter discs at 350 MPa for 10 minutes. The pressed samples were placed in a furnace for sintering at an elevated temperature of 1500°C for two hours with a heating rate of 10°C/min. The group samples were then gradually cooled until they reached the laboratory temperature; the cooling rate of the sample was 10 °C/min. After the green samples were dried, the density of the calcified body was determined using Archimedes' principle by immersion in distilled water. To estimate the density of any sort of sintered sample and the change in density, at least six samples were taken into account.

Using Archimedes' principle, the density of the calcified body was determined in this experiment by immersion in distilled water. According to Eq. (1), the link between apparent density and theoretical density was used to calculate the relative density (r), whereas porosity (ϵ) was calculated using Eq. (2):

$$\rho r = \rho ab / \rho t \quad (1)$$

$$\epsilon = 1 - \rho r \quad (2)$$

TABLE 1. Composition ratios of samples.

Samples	Al ₂ O ₃	MWCNTs
A (pure)	100 wt.%	0 wt.%
A3	97 wt.%	3 wt.%
A5	95 wt.%	5 wt.%

2.2. Sample Consolidation and Sintering

Al₂O₃-MWCNT composites were chosen for consolidation using pressure-free sintering

methods. The samples included pure Al₂O₃ as well as Al₂O₃ 3wt. %, and 5wt. % MWCNT composites. Green pellets were prepared for the traditional sintering process in a uniaxial pressing machine with a load of 395 MPa. Samples were fired to a temperature of 1500°C for 10 minutes at a rate of 10°C/min, then allowed to cool naturally in the furnace until they reached laboratory temperature.

Using Archimedes' approach, the bulk density of the different composites was determined. Al₂O₃ was supposed to have a density of 3.95 g/cm³, while MWCNT was believed to have a density of 2.6 g/cm³. The morphology of the fabricated composite samples was examined using SEM.

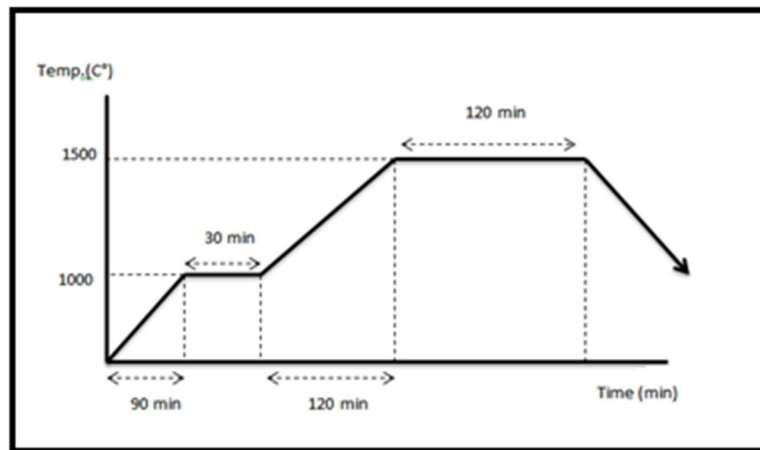


FIG. 1. Sintering furnace program cycle.

2.3. Characterization Techniques

The Al₂O₃ and Al₂O₃-MWCNT powder mixtures, as well as the produced composites, were characterized using X-ray diffraction (XRD) and an electron microscope with field emission scanning (FESEM). The morphologies of the blended powder mixtures were examined using a scanning electron microscope (SEM).

2.4. Mechanical Tests

Hardness measurements of the sintered samples - A (pure Al₂O₃), A3 (3wt% MWCNTs), and A5 (5wt% MWCNTs) - were conducted on polished cross-sections using a Vickers hardness tester, with a 500-gram load applied for 10 seconds. Five indentations were made on each sample to obtain average hardness values. The sintered samples typically had dimensions of 10 mm × 10 mm × 55 mm.

To assess the fracture toughness of the composite materials, the single-edge notched beam method was used. Each sample had a grooved incision, and the absorbed energy was measured through an impact test. Toughness values were then calculated using the following equations [22]:

$$IE = l * \omega [\cos(\alpha) - \cos(\beta)] \quad (3)$$

where **IE** is impact energy absorbed by damage sample, **l** = 0.75m is length of the arm, **ω** = 25.81 kg is the weight of the mass, **α** = 141.5°, and **β** is computed angle from test.

The toughness was then determined using the equation:

$$\text{Toughness} = IE/a \quad (4)$$

where **a** represents the cross-sectional area of the sample.

3. Results and Discussion

3.1. Structural Characterization

The XRD patterns are shown in Fig. 2. The majority of the sintered samples consisted of α-Al₂O₃. All samples had high-intensity patterns. The high-intensity peaks of the XRD patterns show that the powder had a high degree of crystallinity. For each prepared sample, the peaks correspond to a single-phase hexagonal lattice (R-3c space group, space group number 167). Specifically, the reference sample (A) matches ICSD: 31546 (Ref. Code 98-003-1546) [23], sample A3 corresponds to ICSD: 75560 (Ref. Code 98-007-5560) [24], and sample A5 aligns with ICSD: 160604 (Ref. Code 98-016-0604) [25]. These peaks confirm the presence of a single phase in each prepared sample, with no

additional minor phases detected, suggesting that the milling process did not introduce any unwanted phase transformations.

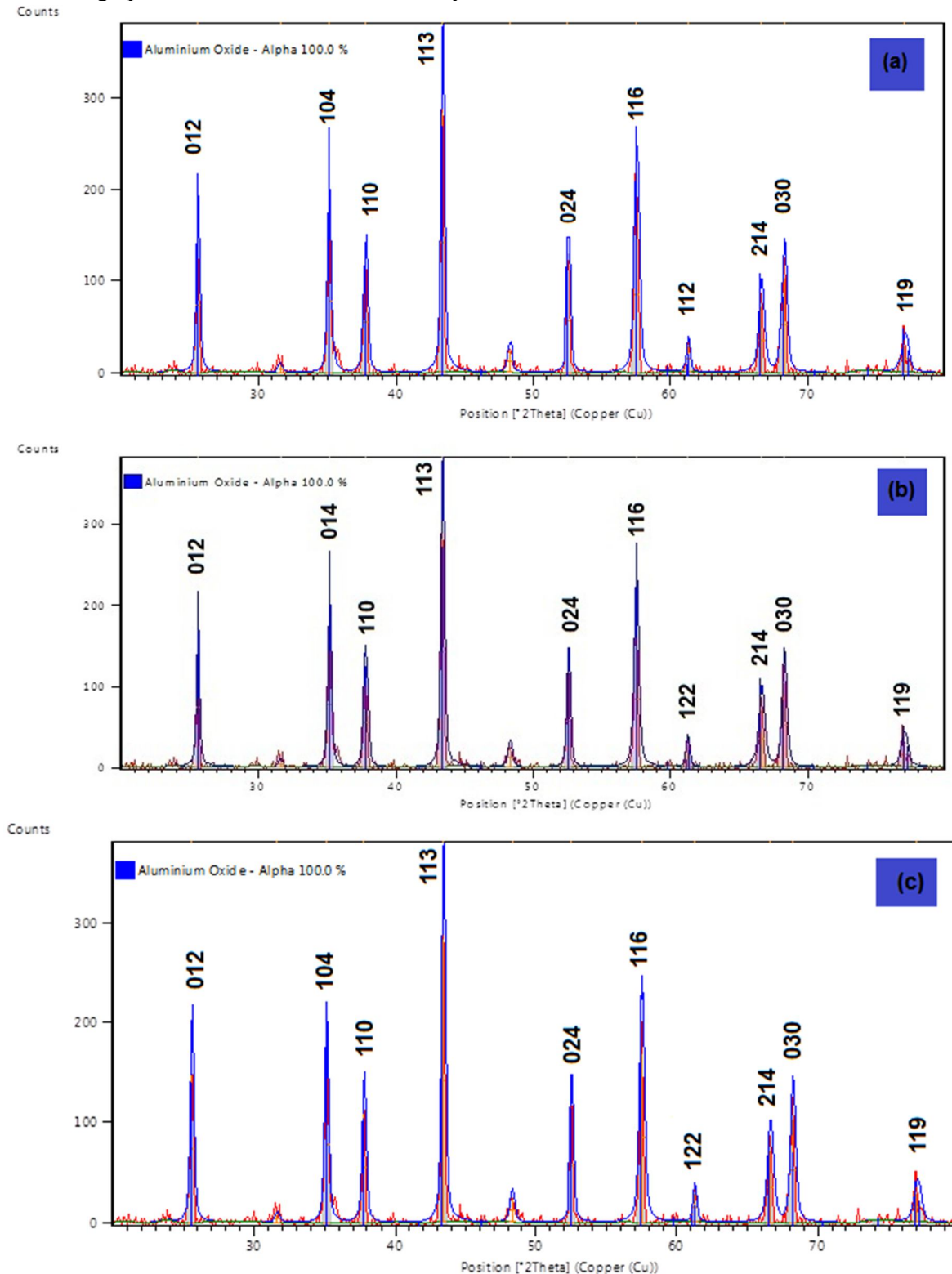


FIG. 2. XRD patterns of the manufactured compositions: (a) A, (b) A3, and (c) A5.

3.2 Analysis of sample morphology

Figures 3(a)-3(b) show the morphology of the multi-walled carbon nanotubes (MWCNTs) reinforcement phase and the alumina (Al₂O₃)

matrix phase. Figure 3(a) presents an SEM image of carbon tubes with diameters ranging from approximately 20 to 26 nm. Figure 3(b) illustrates a homogeneous alumina ceramic. It demonstrates consistency in the structure of the

ceramic particles, which are mostly uniform, with an average grain size of 6 μm , while

discernible porosity between the grains is also observed.

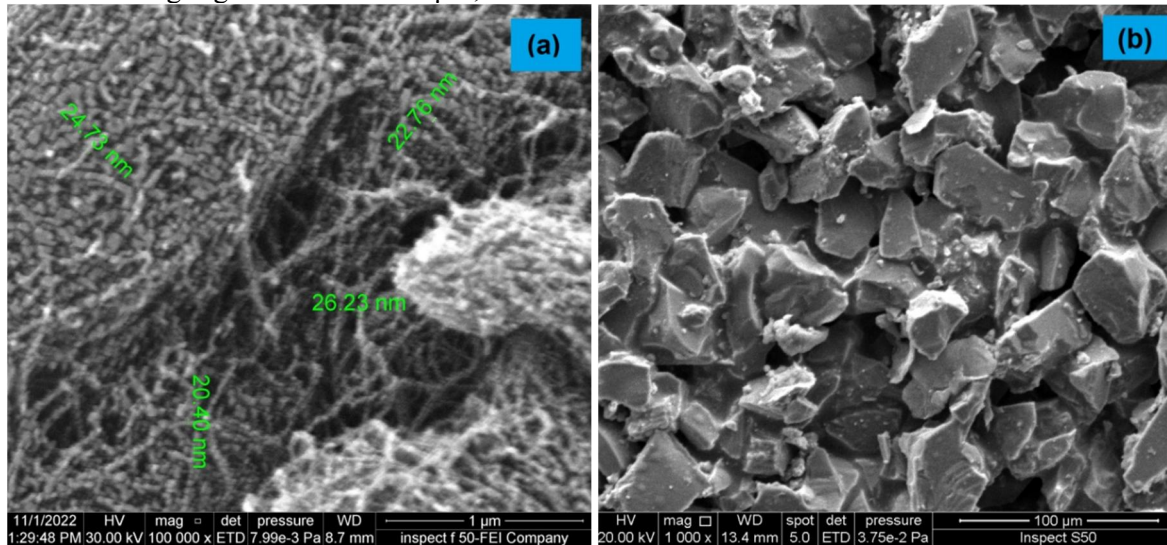


FIG. 3. SEM images of (a) MWCNTs and (b) Al_2O_3 .

Figures 4(a) and 4(b) show the microstructures of monolithic alumina ceramics. Image (a) corresponds to the pure sample. The particle size analysis of the monolithic sample (A) indicates that the ceramic grain sizes are mostly equivalent, with an average grain size of 6 μm . Figure 4 presents SEM images of the surfaces of particles smaller than 6 μm in size for (a) the pure sample (0.0 wt.% MWCNTs). The images in (a) and (b) reveal surface morphologies associated with intergranular fracture, transgranular fracture, and plastic deformation. Alumina fragments with a size of less than 6 μm were discovered to have a faceted

structure with sundry sharp corners, as seen in Figs. 4(a) and 4(b). These fragments had rough surfaces and a morphology that was primarily broken. According to the FESEM images in Figure 4(b), the observed fractures are primarily intergranular, with localized transgranular fractures [26]. Quasi-static Vickers indentation tests confirm the mixed-mode nature of crack propagation in ceramics under ballistic conditions [21]. Additionally, fragmented regions within the ceramics show traces of minute smearing, indicating significant underlying plastic deformation.

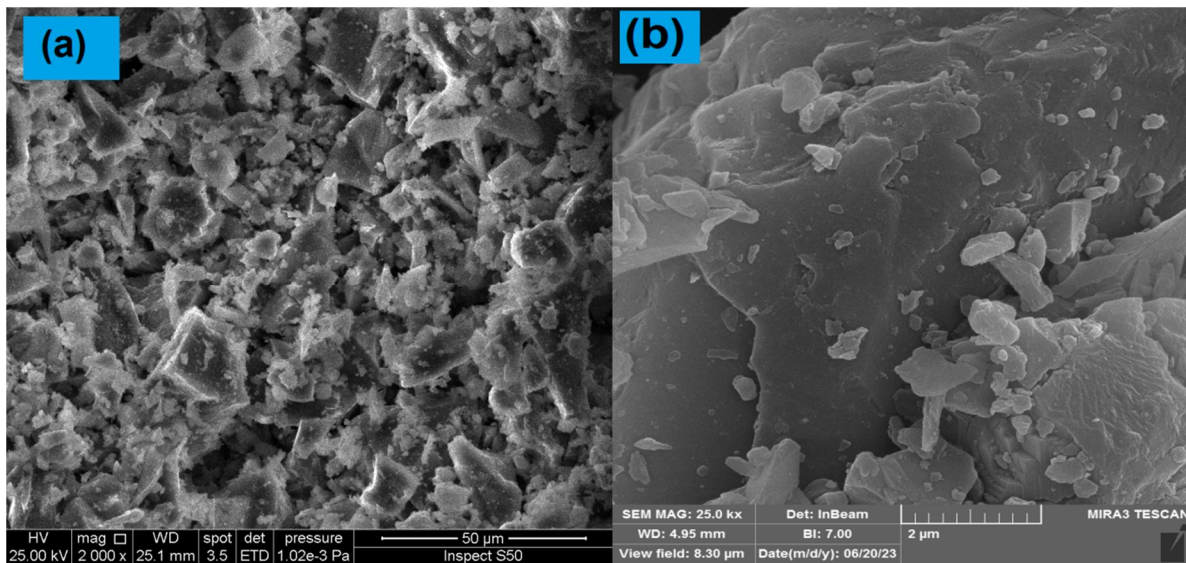


FIG.4. FESEM and SEM micrographs of fracture surfaces: (a) SEM of A sample, (b) FESEM of A sample.

The micrographs of fractured surfaces for the nanocomposite A3 (alumina with a 3 wt.% MWCNT addition) acquired by SEM and

sintered at 1500 $^{\circ}\text{C}$ are shown in Fig. 5. The sample had good carbon nanotube dispersion, but it was also possible to see that the A3 sample

developed a nonhomogeneous morphology. Compared to the A5 samples, the MWCNT in the samples appear to be more evenly distributed. This improved dispersion may contribute to the enhanced mechanical properties of the nanocomposite [27]. The presence of MWCNTs at the grain boundaries is indicated by black arrows in the micrographs. Micrographs of the composition A3 (Al_2O_3+3 wt. % MWCNT) sintered at 1500°C are shown in the figures. Although the sample had low densification and a lower density than the previous sample after sintering at 1500°C , carbon nanotubes are still visible at the grain boundaries. Figure 5 shows SEM images of the fracture surface for sample A3, where all specimens exhibit highly textured fracture surfaces with numerous dimpled

patterns [28]. The average dimple size remained relatively unchanged with increasing nanotube concentration.

Although minor local agglomerates of MWCNTs are observed in some regions, the majority of the fracture surface is covered with well-dispersed individual nanotubes. As the MWCNT concentration increased, so did the presence of individual nanotubes on the fracture surface. Most MWCNTs appear as fractured segments, indicating that they ruptured during the fracture process. Additionally, increased surface roughness is evident due to the formation of several "bulge" regions. These bulges consist of a few broken MWCNTs that are fully embedded within the surrounding matrix [29].

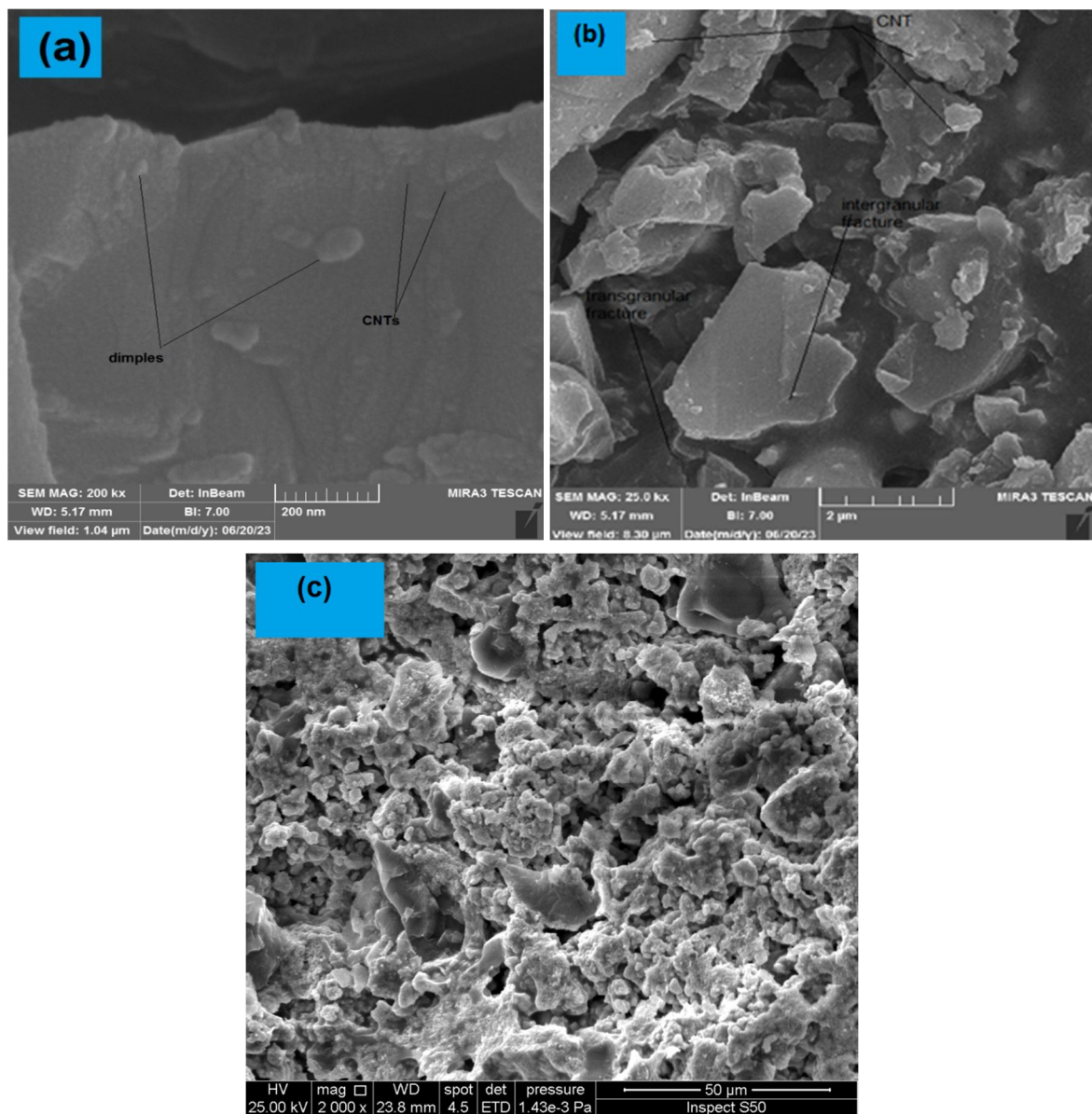


FIG. 5. FESEM and SEM micrographs of fracture surfaces: (a) and (b) FESEM of A3 sample, (c) SEM of the same sample.

The micrographs of the composition A5 (Al_2O_3+5 wt.% MWCNT) sintered at 1500°C are shown in Figs. 6(a), 6(b), and 6(c). A relative increase in porosity is observed due to the increase in the amount of CNTs in the matrix. When MWCNT was added, the grain development was stopped, leading to isolated concentrations of carbon nanotubes in the microstructure. Compared to the A3 sample, MWCNTs are found to agglomerate. The observed decrease in the hardness and toughness of this nanocomposite could be attributed to this non-uniform dispersion.

Furthermore, the densification of alumina nanocomposites was significantly affected by the addition of MWCNTs within a tolerable range. The more even distribution of MWCNTs in alumina nanocomposites helped hinder the carbothermal reduction of alumina. Most MWCNTs exhibited broken segments, indicating that they ruptured during the fracture. The micrographs also reveal increased surface roughness due to the formation of multiple newly formed "bulge" regions [29].

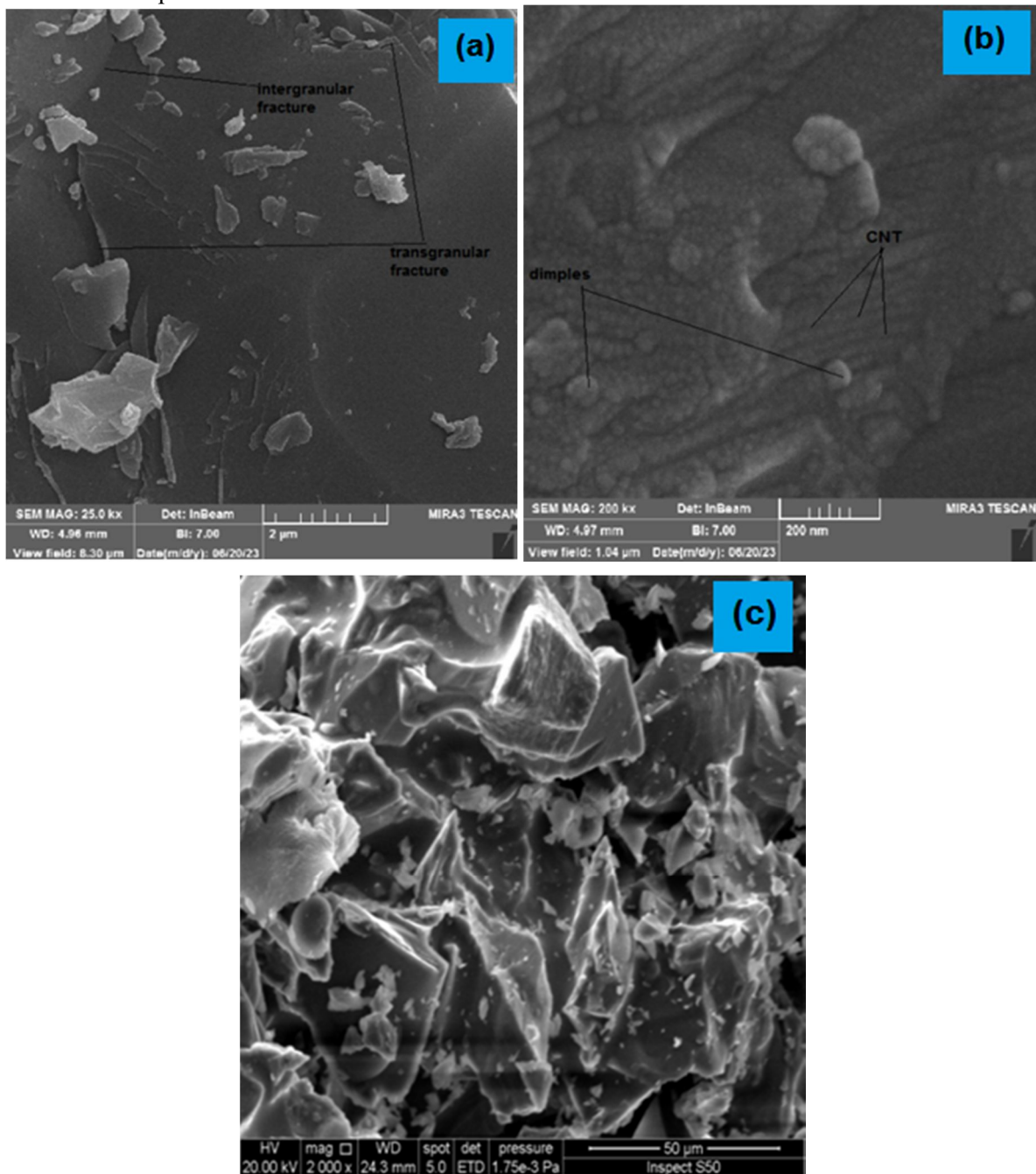


FIG. 6. FESEM and SEM micrographs of fracture surfaces: (a) and (b) FESEM of A5 sample, (c) SEM of the same sample.

In the context of ceramics composites for armor applications, "bulge" locations refer to specific regions on the surface of the alumina matrix where a noticeable deformation or protrusion occurs. These bulges can appear when high ratios of MWCNTs are incorporated into the ceramic composite.

The formation of these bulges is typically associated with localized changes in the microstructure or mechanical properties of the composite. When MWCNTs are added to the ceramic matrix, especially at high concentrations, they can interact with the surrounding material in a way that leads to the development of these bulging regions. Several factors may contribute to their formation:

1. Entanglement and Clustering: MWCNTs have a tendency to entangle and cluster together due to strong van der Waals forces and their unique sp² bonding. When these clusters are embedded within the ceramic matrix, they can create regions of increased volume or local strain, which can lead to bulges on the surface [29].
2. Differential Stress: The incorporation of MWCNTs can introduce areas of differential stress within the composite. Depending on the distribution and orientation of MWCNTs, certain regions may experience more stress than others, resulting in localized deformation and bulging [31].
3. Interfacial Effects: The interaction between MWCNTs and the ceramic matrix can influence how stresses are distributed. Variations in the strength of the interfacial bonding between the MWCNTs and the matrix can lead to uneven mechanical responses, potentially causing bulging [32].
4. Thermal Effects: During processing or post-processing, variations in temperature or differences in thermal expansion coefficients between MWCNTs and the ceramic matrix can create localized thermal stress, which may contribute to the formation of bulges [33].

TABLE 2: Apparent density, theoretical density, relative density, porosity, and mean pore diameter of the sintered samples.

Composition	A	A3	A5
Apparent density ($\rho_{ab}, \text{g.cm}^{-3}$)	3.75	3.78	3.8
Theoretical density ($\rho_t, \text{g.cm}^{-3}$)	3.99	3.98	3.96
Relative density ($\rho_r, \%$)	93.98	94.97	95.95
Porosity ($\varepsilon, \%$)	0.74	0.51	0.43
Mean pore diameter (nm)	8.72	8.26	4.76

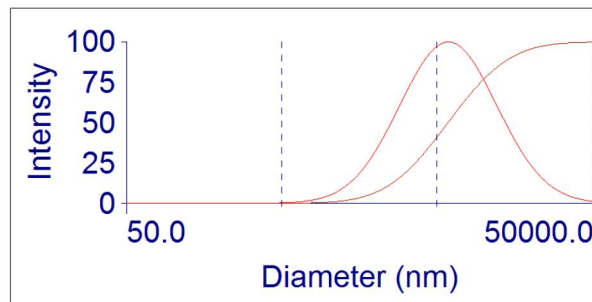


FIG. 7. Particle size distributions (PSDs).

Using dynamic laser scattering, the particle size distribution (PSD) of pure Al₂O₃ powder mixtures was determined, and the zeta potential was utilized to assess the dispersion state. The average particle size of the different powder mixtures was ascertained by calculating the PSD of Al₂O₃ powder mixtures. The average size of the Al₂O₃ particles is approximately 5.8 μm, as indicated by the PSD of pure Al₂O₃ shown in Fig. 6. It is noteworthy that the pure Al₂O₃ obtained had a particle size of around 25 μm.

This demonstrates that Al₂O₃ particles can be ground to an extremely fine size in a short amount of time during milling.

The analysis of Fig. 7 relates to several aspects of the composite, where the distribution of particle sizes, especially in composite materials, is a critical factor that affects the overall material properties and performance. A well-controlled, narrow distribution can lead to more uniform and enhanced properties, making

it an important consideration in materials science and engineering.

1. The size distribution: The average particle size of 5.887 μm refers to the average Al_2O_3 particle size, and the actual particle sizes can vary [34].
2. The width of distribution: The width of the particle size distribution is a key factor. A narrow distribution means that most particles are close in size to the average. In contrast, a broad distribution means that particles can vary greatly in size. The distribution width can affect properties such as packing density, sintering behavior, and mechanical properties of the composite [34].
3. Effect on composite properties: When Al_2O_3 particles are combined with carbon nanotubes (MWCNTs), the particle size distribution of both components is critical. A narrow distribution can help ensure more consistent and predictable properties in the composite. If both Al_2O_3 and MWCNT have narrow size distributions, it could lead to better particle packing, uniform dispersion, and possibly improved mechanical properties [35].
4. Effect on sintering: During the sintering process, the particle size distribution can affect how the particles pack together. A tighter distribution may result in more efficient packing and improved sintering, leading to a denser and stronger composite [36].
5. Homogeneity: In composite materials, achieving a homogeneous distribution of components is essential. A tight particle size distribution can help achieve this uniformity, preventing issues such as phase separation and particle aggregation during mixing and processing [37].

After consolidation by traditional sintering, Table 2 displays the relative density and porosity of monolithic alumina and MWNT/ Al_2O_3 composites. The relative densities were discovered to be between 93% and 95%. It is implied that MWNTs encourage densification in these materials by the rise in relative density of MWNT/ Al_2O_3 composites with increasing carbon nanotube concentration. As expected, the relative density decreased with increasing Al_2O_3 content under the same sintering temperature and holding time. Additionally, sample A (pure) had larger particles than the other samples, which prevented the particles from fitting as well and

resulted in higher porosity in the compact. The enhanced sintering ability may be attributed to the efficient diffusion layer that connects the MWCNTs and the alumina grains. Depending on the sintering temperature, an aluminum oxy-carbide phase (Al-O-C interphase between MWNTs and Al_2O_3 grains) may form [38,39].

3.3. Mechanical Tests

Vickers hardness values for sintered samples are shown in Table 3. Despite variations in porosity, the compositions of the samples under investigation were in good agreement with Karandikar's measurements [40]. For ballistic applications, where it is anticipated that the projectile will be ruptured by the ballistic tile, the hardness attribute is crucial. The MWCNT particles in the Al_2O_3 matrix, as shown by the experimental results, enhanced the mechanical strength of the nanocomposite, as shown by the hardness and toughness results. The hardness and toughness of the nanocomposites were improved by adding up to 3 wt.% more MWCNT to the alumina matrix (Al_2O_3) [41]. A higher MWCNT cluster content in the nanocomposite structure may explain why exceeding this content did not significantly improve hardness and toughness [42].

TABLE 3. Vickers hardness of sintered compositions.

Compositions	HV
A	370.3
A3	763.8
A5	661.6

Table 4 presents the impact energy of the damaged core for each of the synthesized samples, revealing that sample A3 (3wt% MWCNTs) exhibited the highest average absorption energy compared to samples A (pure Al_2O_3) and A5 (5wt% MWCNTs).

TABLE 4. Impact energy (Kg.m)

Compositions	I.E (impact energy for all synthesized samples)
A	1.43
A3	1.94
A5	1.64

TABLE 5. Toughness (impact energy absorbed per unit damage area) (kg.m/cm^2)

Compositions	Toughness
A	1.4721
A3	2.08
A5	1.2632

The toughness values for the examined samples are shown in Table 5. The toughness and strength values of each composition varied. However, compared to composition samples A (pure) and A5, composition sample A3 showed nearly the greatest average values of toughness strength. Due to cracks and effective MWCNT dispersion in the Al₂O₃ matrix, the addition of carbon nanotube MWCNTs to the Al₂O₃ ceramic significantly improved its toughness and, consequently, Al₂O₃ matrix composites fracture toughness.

4. Conclusions

In this work, three commercial alumina compositions—designated A3, A5, and A—were examined as ballistic ceramics. These compositions consisted of Al₂O₃ with 3 wt.%, 5 wt.%, and 0 wt.% MWCNTs, respectively. Compositions were examined using X-ray diffraction (XRD), scanning electron microscope (SEM), and mechanical testing. Vickers hardness

measurements and the Charpy impact test were used to assess the toughness of the samples.

Among the compositions, A3 was selected for ballistic testing due to its superior hardness and toughness. The addition of MWCNTs significantly improved the mechanical properties of the A3 alumina nanocomposite by enhancing densification, inhibiting excessive grain growth, reinforcing the matrix, and increasing both hardness and fracture toughness. Among the investigated nanocomposites, the Al₂O₃/3 wt.% MWCNT nanocomposite exhibited the lowest porosity, the smallest grain size, and the highest mechanical performance in terms of flexural strength and fracture toughness. It was also sintered at 1500 °C.

The conventional ceramic processing method used to fabricate alumina nanocomposites with 3 wt.% MWCNTs demonstrated significant potential for ballistic shielding applications.

References

- [1] Sharma, N., Saxena, T., Alam, S.N., Ray, B.C., Biswas, K., and Jha, S.K., *Mater. Today Commun.*, 31 (2022) 103764.
- [2] Ighodaro, O.L. and Okoli, O.I., *Int. J. Appl. Ceram. Technol.*, 5 (3) (2008) 313.
- [3] Rathinavel, S., Priyadharshini, K., and Panda, D., *Mater. Sci. Eng. B*, 268 (2021) 115095.
- [4] Fang, H., Gao, J.F., Wang, H.T., and Chen, C.S., *J. Memb. Sci.*, 403 (2012) 41.
- [5] Mondal, K., Nuñez III, L., Downey, C.M., and Van Rooyen, I.J., *Ind. Eng. Chem. Res.*, 60 (17) (2021) 6061.
- [6] Zuccarini, C., Ramachandran, K., Russo, S., Jayakody, Y.C., and Jayaseelan, D.D., *Int. J. Ceram. Eng. Sci.*, 5 (1) (2023) e10168.
- [7] Palmero, P., *Nanomaterials*, 5 (2) (2015) 656.
- [8] Heimann, R.B., "Classic and Advanced Ceramics: From Fundamentals to Applications". (John Wiley & Sons, 2010).
- [9] Gao, C., Feng, P., Peng, S., and Shuai, C., *Acta Biomater.*, 61 (2017) 1.
- [10] Mu, X. N. et al., *Mater. Sci. Eng. A*, 687 (2017) 164.
- [11] Thirugnanasabandam, A., Ramachandran, K., Mariadas, A., Jayaraman, J.T., Boddula, R., and Jagannathan, M., *Curr. Anal. Chem.*, 17 (6) (2021) 849.
- [12] Sharma, N., Syed, A.N., Ray, B.C., Yadav, S., and Biswas, K., *J. Asian Ceram. Soc.*, 7 (1) (2019) 1.
- [13] Cho, S. et al., *Compos. Part A Appl. Sci. Manuf.*, 139 (2020) 106138.
- [14] Chen, B., Kondoh, K., Umeda, J., Li, S., Jia, L., and Li, J., *J. Alloys Compd.*, 789 (2019) 25.
- [15] He, P. et al., *J. Alloys Compd.*, 819 (2020) 153009.
- [16] Vasiliev, A.L. and Padture, N.P., *Scr. Mater.*, 56 (6) (2007) 461.
- [17] Choudhary, M., Sharma, A., Aravind Raj, S., Sultan, M.T.H., Hui, D., and Shah, A.U.M., *Nanotechnol. Rev.*, 11 (1) (2022) 2632.
- [18] Cygan, T. et al., *Ceram. Int.*, 46 (6) (2020) 7170.
- [19] Silva, M.V., Stainer, D., Al-Qureshi, H.A., Montedo, O.R.K., and Hotza, D., *J. Ceram.*, 2014 (2014) 1.

- [20] Wei, T., Fan, Z., Luo, G., and Wei, F., *Mater. Lett.*, 62 (4–5) (2008) 641.
- [21] Zhu, Y., “Development of Alumina-based Ceramic Nanocomposites for Armour Applications”, (Loughborough University, 2017).
- [22] González-Velázquez, J.L., "Mechanical Behavior and Fracture of Engineering Materials", (Springer, 2020).
- [23] Cox, D.E., Moodenbaugh, A.E., Sleight, A.W., and Chen, H.Y., *Spec. Publ.*, 567 (1980) 189e201.
- [24] Sawada, H., *Mater. Res. Bull.*, 29 (2) (1994) 127.
- [25] Kondo, S., Tateishi, K., and Ishizawa, N., *Jpn. J. Appl. Phys.*, 47 (1S) (2008) 616.
- [26] Huang, L., Yao, W., Mukherjee, A.K., and Schoenung, J.M., *J. Am. Ceram. Soc.*, 95 (1) (2012) 379.
- [27] Ahmad, I. et al., *Compos. Sci. Technol.*, 70 (8) (2010) 1199.
- [28] Nasresfahani, M.R. and Shamanian, M., *J. Mater. Sci.*, 53 (15) (2018) 10812.
- [29] Sharma, N., Syed, A.N., Ray, B.C., Yadav, S., and Biswas, K., *J. Asian Ceram. Soc.*, 7 (1) (2019) 1.
- [30] Sharma, N., Saxena, T., Alam, S.N., Ray, B.C., Biswas, K., and Jha, S.K., *Mater. Today Commun.*, 31 (2022) 103764.
- [31] Liu, Y. et al., *Nanotechnol. Rev.*, 9 (1) (2020) 190.
- [32] Yang, Q., Kalathiparambil, K., Elg, D.T., Ruzic, D., and Kriven, W.M., *Acta Mater.*, 132 (2017) 479.
- [33] Krause, B. et al., *Carbon*, 48 (10) (2010) 2746.
- [34] Sharma, N., Syed, A.N., Ray, B.C., Yadav, S., and Biswas, K., *J. Asian Ceram. Soc.*, 7 (1) (2019) 1.
- [35] Hanzel, O. et al., *J. Eur. Ceram. Soc.*, 35 (5) (2015) 1559.
- [36] Sarkar, S. and Das, P.K., *Ceram. Int.*, 40 (2014) 7449.
- [37] Sarkar, S. and Das, P.K., *Mater. Chem. Phys.*, 137 (2012) 511.
- [38] Sheikh, S. et al., *Int. J. Ref. Metals. Hard Mater.*, 49 (2015) 153.
- [39] Heimann, “Classic and Advanced Ceramics: From Fundamentals to Applications”, (Wiley-VCH, New York, NY, USA, 2010).
- [40] Ramachandran, K. et al., *J. Mater. Res. Technol.*, 24 (2023) 6595.
- [41] Ghahramani, P., Behdinan, K., Moradi-Dastjerdi, R., and Naguib, H.E., *Nanotechnol. Rev.*, 11 (1) (2021) 55.
- [42]